Polymer depletion-driven cluster aggregation and initial phase separation in charged nanosized colloids

Christoph Gögelein, Gerhard Nägele, Johan Buitenhuis, Remco Tuinier, and Jan K. G. Dhont

Citation: The Journal of Chemical Physics **130**, 204905 (2009); doi: 10.1063/1.3141984
View online: https://doi.org/10.1063/1.3141984
View Table of Contents: http://aip.scitation.org/toc/jcp/130/20
Published by the American Institute of Physics

Polymer depletion-driven cluster aggregation and initial phase separation in charged nanosized colloids

Christoph Gögelein,[1,a)] Gerhard Nägele,[1] Johan Buitenhuis,[1] Remco Tuinier,[2] and Jan K. G. Dhont[1]
[1]*Institut für Festkörperforschung, Forschungszentrum Jülich, D-52425 Jülich, Germany*
[2]*DSM Research, ACES, 6160 MD Geleen, The Netherlands*

(Received 9 February 2009; accepted 1 May 2009; published online 28 May 2009)

We study polymer depletion-driven cluster aggregation and initial phase separation in aqueous dispersions of charge-stabilized silica spheres, where the ionic strength and polymer (dextran) concentration are systematically varied, using dynamic light scattering and visual observation. Without polymers and for increasing salt and colloid content, the dispersions become increasingly unstable against irreversible cluster formation. By adding nonadsorbing polymers, a depletion-driven attraction is induced, which lowers the stabilizing Coulomb barrier and enhances the cluster growth rate. The initial growth rate increases with increasing polymer concentration and decreases with increasing polymer molar mass. These observations can be quantitatively understood by an irreversible dimer formation theory based on the classical Derjaguin, Landau, Verwey, and Overbeek pair potential, with the depletion attraction modeled by the Asakura–Oosawa–Vrij potential. At low colloid concentration, we observe an exponential cluster growth rate for all polymer concentrations considered, indicating a reaction-limited aggregation mechanism. At sufficiently high polymer and colloid concentrations, and lower salt content, a gas-liquidlike demixing is observed initially. Later on, the system separates into a gel and fluidlike phase. The experimental time-dependent state diagram is compared to the theoretical equilibrium phase diagram obtained from a generalized free-volume theory and is discussed in terms of an initial reversible phase separation process in combination with irreversible aggregation at later times.
 [DOI: 10.1063/1.3141984]

I. INTRODUCTION

Mixtures of colloids and polymers show interesting equilibrium and nonequilibrium phase behavior.[1] In thermal equilibrium, the system may macroscopically phase separate into a dilute fluid and a dense fluid or crystalline colloid phase.[2] This is similar to coexisting gas and liquid or crystalline phases in molecular systems. However, in many situations, colloid-polymer mixtures form dynamically arrested colloidal structures out of equilibrium such as clusters, gels, or glasses. Gels and glasses are noncrystalline, solidlike, and long-living macroscopic structures. Equilibrium and nonequilibrium processes have been studied in the past mainly as two well distinct phenomena. However, more recent experiments on colloid-polymer mixtures point to a connection between the spinodal line of the equilibrium phase diagram and the gelation boundary.[3–7] In fact, strong evidence has been given that spinodal decomposition induces gelation in neutral colloid-polymer mixtures with small polymer-to-colloid size ratios q.[8] Whether the onset of gelation is governed by equilibrium phase separation also at larger q, and for charged colloids at low salinity, has not been explored to date.

Using mode-coupling theory, attempts have been made to explain the gelation process in dense systems by a dynamical arrest.[9,10] Recently, a kinetic model was used to study the link between gas-liquid demixing and cluster aggregation phenomena for low colloid volume fractions.[11] However, no common understanding or overall theoretical description explaining the gelation process has been achieved to date.[12]

In this work, we investigate the aggregation and demixing of mixtures of nanosized Ludox silica particles and dextran polymers in (salty) water. The colloidal particles interact by a short-ranged van der Waals (vdW) attraction and a screened Coulomb repulsion. By varying the salt concentration, we have tuned the Coulomb repulsion and thus, the colloid cluster aggregation rate. The polymer chains add an additional effective attraction to the colloids by the well-known depletion mechanism.[13–15] The range of the depletion-induced attraction can be tuned by the polymer molar mass. We focus here on the effect of long-ranged depletion-induced attractions, where $0.49 \leq q \leq 2.6$. For these q-values a (stable) gas-liquid phase coexistence appears in equilibrium. Thus, our system offers the opportunity to study systematically the interplay between phase separation and cluster aggregation of charged colloids by varying the salt and polymer concentrations, c_s and c, respectively, and the colloid volume fraction ϕ. In our system, the gas-liquid demixing is mainly caused by the polymer-induced depletion attraction, whereas the cluster aggregation is induced by the vdW forces.

Using dynamic light scattering (DLS), we study the ini-

[a)]Electronic mail: c.goegelein@fz-juelich.de.

tial aggregation of dimers as quantified by the collective diffusion coefficient from which the time-dependent cluster size and the cluster growth rate are deduced. The macroscopic phase behavior as a function of c_s, c and ϕ are studied by visual inspection. The onset of aggregation is quantified and analyzed using a dimer formation theory of initial flocculation based on the Derjaguin, Landau, Verwey, and Overbeek (DLVO) pair potential and the Asakura–Oosawa–Vrij (AOV) polymer-induced depletion potential. The effective colloid charge entering the electrostatic part of the pair potential is the only unknown parameter, which we determine by matching the calculated aggregation rate to the experimental one, for systems without added polymers. This yields an overall good description of our experimental observations also in the case of added polymers. The time-dependent macroscopic state diagrams at lower salinity are compared to equilibrium phase diagram calculations for a corresponding model system without vdW attraction, using a recently derived extended generalized free-volume theory (GFVT).[16] As we shall discuss, this comparison points to an interpretation of the experimental state diagrams in terms of an initially reversible phase separation interfering with a slower aggregation process. To our knowledge, the present work is the first quantitative experimental-theoretical study of aggregation and phase behavior in mixtures of nanosized charged colloids and neutral nonadsorbing polymers, where the polymer-colloid size ratio extends up to 2.6.

Previous experiments explored the stability against cluster aggregation of mixtures of larger charged colloids (latex spheres) and polyelectrolytes chains for small values $q \lesssim 0.3$, where no stable gas-liquid phase coexistence occurs.[17–21] Since the polymer radius of gyration in polyelectrolytes solutions depends strongly on the salt content, a quantitative description of the depletion-induced attraction is complicated in these mixtures. In other experimental work, the colloid aggregation in mixtures of sterically stabilized latex spheres and neutral polymer chains was investigated for small values of q.[22–24] In these earlier experiments, an enhanced colloid aggregation rate was observed for increasing polymer concentration and decreasing molar mass. The data were qualitatively discussed in terms of a simpler dimer formation theory where hydrodynamic interactions (HIs) between colloids have been neglected. Petekidis *et al.*[25] investigated the phase behavior and the kinetics of mixtures of charged colloids (latex spheres) and wormlike micelles. Their work was concentrated mainly on the aging (collapse) of the gel, formed at sufficiently high surfactant and salt concentrations.

Our paper is organized as follows: Sec. II gives the essentials of the dimer formation theory of Brownian flocculation with depletion attraction included, and the GFVT of equilibrium phases. Section III includes the sample characterization and describes the evaluation of the DLS data. Our results are described in Sec. IV. In this section, using DLS and dimer formation theory, we study first polymer-free silica dispersions as a function of added salt and colloid concentration (Secs. IV B–IV D). In Secs. IV E and IV F, the influence of added polymers is studied, for fixed colloid and salt concentrations, depending on the polymer concentration and the polymer-to-colloid size ratio. In Sec. IV G, the time-dependent state diagrams of silica-dextran mixtures are studied at low salt concentration, and compared to the predictions of the GFVT. Finally, our conclusions are contained in Sec. V.

II. THEORY

A. DLVO-type description of aggregation kinetics

A colloidal dispersion can be stabilized against aggregation by a sufficiently strong electrostatic repulsion. This is made possible by the fact that the vdW attraction acts only at interparticle distances typically of the order of about 10% of the particle diameter. The vdW effective potential between two dispersed spheres is approximately described by[26]

$$u_{\mathrm{vdW}}(r) = -\frac{A_H}{6}\left(\frac{2a^2}{r^2-4a^2}+\frac{2a^2}{r^2}+\ln\left[1-\frac{4a^2}{r^2}\right]\right), \tag{1}$$

for $r>2a$. Here, r is the center-to-center distance, a is the radius of a colloidal sphere, and A_H is the Hamaker constant. The vdW potential decays as $u_{\mathrm{vdW}}(r)\sim -1/r^6$ for large r, and diverges as $u_{\mathrm{vdW}}(r)\sim -(r-2a)^{-1}$ near contact distance $r=2a$.[27] In the classical DLVO theory, the screened electrostatic interparticle repulsion is described by the effective pair potential

$$\beta u_{\mathrm{el}}(r) = \frac{Z_{\mathrm{eff}}^2 l_B}{(1+\kappa a)^2}\frac{\exp[-\kappa(r-2a)]}{r}, \tag{2}$$

for $r>2a$, with $1/\beta=k_BT$, Bjerrum length $l_B=e^2/(4\pi\varepsilon_0\varepsilon k_BT)$, effective number of elementary charges, Z_{eff}, on the colloidal surface, and the Debye screening parameter κ, with

$$\kappa^2 = 4\pi l_B\left(|Z_{\mathrm{eff}}|\frac{\phi}{v_0}+2\frac{N_A}{M_s}c_s+\frac{N_A}{M_b}c_b\right). \tag{3}$$

Here, $v_0=(4\pi/3)a^3$ is the colloid volume, N_A is Avogadro's number, and M_s and M_b are the salt and buffer molar masses, respectively. The buffer concentration (mass per volume) is denoted by c_b. The strength of the electrostatic potential part is quantified by the contact value $\beta\epsilon=Z_{\mathrm{eff}}^2 l_B/[(1+\kappa a)^2 2a]$. The total pair potential of charged colloids in an electrolyte solution consists thus of the hard-sphere potential, $u_{\mathrm{hs}}(r)$, describing the excluded volume interaction of two spheres of diameter $2a$, the vdW attraction part, $u_{\mathrm{vdW}}(r)$, and the contribution $u_{\mathrm{el}}(r)$ describing the screened electrostatic repulsion arising from overlapping electric double layers,

$$u_{\mathrm{DLVO}}(r) = u_{\mathrm{hs}}(r)+u_{\mathrm{vdW}}(r)+u_{\mathrm{el}}(r). \tag{4}$$

In this paper, the onset of the colloidal aggregation is described by the dimer formation theory of Brownian flocculation.[26,28] Here, the characteristic time for doublet formation is estimated to

$$\tau_a = \frac{\pi\eta a^3}{\phi k_BT}W, \tag{5}$$

where W is the stability ratio, obtained from

$$W = 2a\int_{2a}^{\infty} \frac{\exp(\beta u(r))}{r^2 G(r)} dr. \tag{6}$$

Here, η is the solvent viscosity. The derivation of Eqs. (5) and (6) is summarized in Appendix. The hydrodynamic function, $G(r)$, in Eq. (6) quantifies the relative mobility of two spheres along their line of centers.[29] If two impermeable and smooth spherical particles approach one another with the velocity, v, the liquid in the gap between the two colloids has to be squeezed out. For $r \to 2a$, the pressure in the liquid gap diverges as $\eta v a/(r-2a)^2$,[30] so that $G(r)$ decays to zero as $(r-2a)/a$. The two-sphere hydrodynamics described by $G(r)$ leads thus to an increase in τ_a. Aggregation is possible because the flux due to the interparticle forces, and thus W, remain finite since the vanishing relative mobility at contact is balanced by the diverging vdW attraction.

B. Depletion-induced cluster aggregation

Adding nonadsorbing polymers induces an attractive colloidal interaction, in addition to the vdW attraction. This so-called depletion interaction can be described at small polymer concentrations by the AOV model. In this simplifying model, the effective depletion pair potential acting between two colloids is given by the product of the osmotic pressure of the polymer solution in the reservoir, Π_p^r, and the excluded volume $V_{ex}(r)$, e.g., $u_{AOV}(r) = -\Pi_p^r V_{ex}(r)$.[13–15] The depletion potential between two colloidal spheres due to the presence of polymers reads[15]

$$\beta u_{AOV}(r) = -\frac{c}{c^*}\frac{(1+q)^3}{q^3}\left(1 - \frac{3r}{4(1+q)a} + \frac{r^3}{16(1+q)^3 a^3}\right), \tag{7}$$

where $2a < r < 2[a+R_g]$. Here, $q = R_g/a$ is the size ratio between the polymer radius of gyration, R_g, and colloid sphere radius. The polymer overlap concentration is estimated by $c^* = 3M/(4\pi R_g^3 N_A)$, where M is the polymer molar mass. The AO model assumes freely overlapping polymers, which are described as phantom spheres of radius R_g. In fact, the dextran solution is close to its θ temperature for the temperature $T = 295$ K set in our experiments.[31] As shown by Gast *et al.*,[2] the AOV model is strictly pairwise additive only for $q < 2/\sqrt{3} - 1 \approx 0.1547$. It follows that using the AOV potential requires, in principle, an infinitely dilute colloidal dispersion for larger q. However, the AOV potential description should still apply for the initial dimer formation process. Effects arising from the nonideality of the polymer solution, which are expected to become important at semidilute polymer concentrations, could be incorporated in an additional step.

The total colloid pair potential, $u(r)$, which enters into our calculation of τ_a through Eqs. (5) and (6), is thus given by

$$u(r) = u_{hs}(r) + u_{vdW}(r) + u_{el}(r) + u_{AOV}(r). \tag{8}$$

Using this $u(r)$, the evaluation of W and τ_a in Eqs. (6) and (5), respectively, is straightforward.

C. Generalized free-volume theory of equilibrium phase diagram

To compare the experimentally observed nonequilibrium phase diagrams in colloid-polymer mixtures at lower salinity with the theoretically predicted equilibrium phase diagram, we employ here a modification of the GFVT described, e.g., in Ref. 16. The original theory addresses mixtures of neutral colloids and polymers in the semigrand canonical ensemble, modeling them as colloidal hard spheres in a system volume V which are in osmotic equilibrium with a reservoir solution of nonadsorbing free polymer chains.[32] Recently, the GFVT has been extended to describe mixtures of weakly charged colloidal particles and neutral polymer chains.[16] Within the extended GFVT, the screened electrostatic colloid repulsion is mapped onto an effective hard-sphere interaction using the leading-order Barker and Henderson expression,[33]

$$a' = a + \frac{1}{2}\int_{2a}^{\infty} dr(1 - \exp[-\beta u_{el}(r)]), \tag{9}$$

where a' is the effective colloid radius. The effective volume fraction, ϕ', is then defined by

$$\phi' = \left(\frac{a'}{a}\right)^3 \phi = m\phi. \tag{10}$$

For the free-volume theory to be applicable, m should be rather close to one [i.e., $m \lesssim 1.225$ (Ref. 34)]. The semigrand canonical free energy density is formulated as

$$\omega(\phi, y) = f(\phi) - \int_0^y \alpha(\phi, \tilde{y}) \frac{\partial \beta \Pi_p^r(\phi, \tilde{y}) v_0}{\partial \tilde{y}} d\tilde{y}, \tag{11}$$

where $y = c/c^*$, and Ω is the semigrand canonical free energy density. Moreover, $f = \beta F v_0/V$ is the normalized free energy density of the hard-sphere reference system. The second term on the right-hand side is the free energy contribution due to the polymers. For polymers in a θ-solvent, the depletion thickness to colloid size ratio is

$$q_s(q, y) = 0.938(q/\sqrt{1 + 5.94y^2})^{0.9}. \tag{12}$$

This expression includes colloid curvature effects. The depletion thickness, h, close to a convexly curved colloid surface is smaller than at a flat wall. The reduced osmotic pressure in a semidilute polymer solution can be approximated by

$$\beta \Pi_p^r(q, y) v_0 = q^{-3}(y + 4.1y^3). \tag{13}$$

The free-volume fraction appearing in Eq. (11), namely, $\alpha(\phi, y)$, is approximated by the scaled-particle theory expression

$$\alpha(\phi, y) = (1-\phi)\exp(-b_1\gamma - b_2\gamma^2 - b_3\zeta - 3b_3\zeta^2 - 3b_3\zeta^3), \tag{14}$$

where $\gamma = \phi/(1-\phi)$, $\zeta = \phi'/(1-\phi')$, $b_1 = 3q_s + 3q_s^2$, $b_2 = 9q_s^2/2$, and $b_3 = q_s^3$. The free energy density of the hard-sphere reference system consists of the ideal gas contribution, and of the excess contribution modeled by the Carnahan–Starling free energy density.[35] The gas-liquid coexistence curve (binodal) follows, for a given polymer reser-

voir concentration, y, from the equality of the osmotic pressure and chemical potential in the gas and liquid phases. Likewise, the spinodal line is calculated from the inflection point of the free energy density, and the critical point follows from its saddle point.

III. EXPERIMENTAL DETAILS

A. Sample materials

Silica particles (Ludox™ TMA) were kindly provided by Grace Davison (Worms, Germany). These amorphous particles were supplied in a de-ionized aqueous stock dispersion of $p\mathrm{H}=6.9$. The dispersion contains a mixture of 5-chloride-2-methyl-2*H*-isothiazol-3-on and 2-methyl-2*H* -isothiazol-3-on with a total volume fraction of 0.0025% to prevent fungal decay and bacterial growth. The mass density of the amorphous silica particles is (2.1 ± 0.1) g/cm^3, and was determined from the weight loss when drying a known amount of dispersion, the colloidal dispersions density, and the density of water.

Dextran from Leuconostoc with molar masses $M=4\times10^4$, 5×10^5, and 2×10^6 g/mol, respectively, was purchased from Fluka. The radius of gyration, R_g, of dextran was estimated, using the results from Ref. 31, as $R_g=0.0633M^{0.427}=(5.8\pm0.4)$, (17 ± 1), and (31 ± 2) nm, respectively, on assuming a polydispersity of 15%. We note that the exponent of $0.427<0.5$ is indicative of a somewhat branched chain structure. The polymer overlap concentration is estimated as $c^*=3M/(4\pi N_\mathrm{A}R_g^3)$, resulting in $c^*=0.0796$, 0.0391, and 0.0265 g/cm^3 for $M=4\times10^4$, 5×10^5, and 2×10^6 g/mol, respectively. The mass density of dextran is 1.637 g/cm^3.[36] To ensure that dextran does not adsorb on the silica-water interface and to increase the colloidal stability, an ammonium-chloride buffer has been used. The buffer concentration, c_b, was set to 0.02 mol/l with $p\mathrm{H}=9.2\pm0.1$, and the ionic strength was varied by adding sodium chloride (Sigma-Aldrich). The aqueous Ludox dispersion was dialyzed against the ammonium-chloride buffer solution for 2 weeks. For all solutions, the aqueous medium was taken from a Millipore ultraclean facility. All solutions where properly sealed to prevent evaporation of the dissolved ammonia. To avoid bacterial growth, *N*-methylisothiazolon-HCl (Chemos, Regenstauf, Germany) was added at a volume fraction of 0.0025%. Furthermore, the silica-containing dispersion was stored in plastic containers to prohibit wall-induced aggregation occurring in glass containers. The samples have been prepared from stock solutions to ensure rapid mixing of the polymer and the colloidal solutions. For this purpose, the dextran powder was dissolved in a buffer solution containing already the desired sodium chloride concentration. Stirring the polymer solution was avoided to prevent disrupting the polymer chains. Shortly before the samples were prepared, the dialyzed Ludox dispersion was mixed with a proper amount of a high concentrated sodium chloride solution (1 mol/l). Afterward, the desired colloid-polymer mixture was prepared by adding proper amounts of the colloidal stock solution, the polymer solution, and the salt-containing buffer solution. The suspension was then gently mixed.

B. Experimental techniques and sample characterization

DLS experiments were performed on an ALV/CGS-8F S/N 060 laser goniometer system (ALV, Langen, Germany), using a 22 mW helium Neon laser (JDS Uniphase, Milpitas, USA) and a single avalanche photodiode detector. The temperature was set to $T=295$ K in all our DLS measurements. Samples containing the colloidal dispersion only were filtered through a 0.45 μm pore-size Nylon filter (Roth, Karlsruhe, Germany) to remove dust. Mixtures of colloids and polymers were filtered with Cameo Nylon filters of pore size 5.0 μm. For DLS measurements, the solutions were filled into cylindrical glass cells (Hellma, Müllheim, Germany) of 10 mm diameter. All samples where sealed with Teflon tape.

1. Colloidal particle size and polymer radius of gyration

The radius of the silica spheres was determined from the measured diffusion coefficient, for various colloid concentrations and at a salt concentration of $c_s=0.15$ mol/l. For each scattering angle, θ, the normalized intensity autocorrelation function,

$$g^{(2)}(t)=\frac{\langle I(0)I(t)\rangle}{\langle I^2(0)\rangle}, \tag{15}$$

was determined. The normalized autocorrelation function of the scattered electric field,

$$g^{(1)}(t)=\frac{\langle \vec{E}^*(t)\cdot\vec{E}(0)\rangle}{\langle|\vec{E}(0)|^2\rangle}, \tag{16}$$

was deduced from the Siegert relation,[37]

$$g^{(2)}(t)=1+[g^{(1)}(t)]^2. \tag{17}$$

In a dilute suspension of uncorrelated monodisperse spherical particles, the field autocorrelation function decays single exponentially according to

$$g^{(1)}(t)=f_c\exp[-(t/\tau)], \tag{18}$$

where $f_c<1$ is the coherence area factor limited by the applied optics.

In a dilute sample, the relaxation time, τ, of density fluctuations of wavelength $2\pi/k$ is related to the single-sphere diffusion coefficient, D_0, by $1/\tau=D_0k^2$, where $k=(4\pi n/\lambda)\sin(\theta/2)$ is the scattering wave number of laser light of vacuum wavelength λ in a medium of refractive index n. Our Ludox particles are not ideally monodisperse so that a superposition of exponential functions is measured. For simplicity, we globally describe this superposition by the Kohlrausch–William–Watts (KWW) stretched-exponential expression,

$$g^{(1)}(t)=f_c\exp[-(t/\tau)^{\beta_\mathrm{KWW}}], \tag{19}$$

with a stretching exponent, β_KWW, that characterizes the overall size polydispersity.[38] The mean relaxation time is then given by $\langle\tau\rangle_\mathrm{KWW}=(\tau/\beta_\mathrm{KWW})\Gamma(1/\beta_\mathrm{KWW})$, where Γ is the gamma function. On plotting $\langle\tau\rangle_\mathrm{KWW}$ versus k^2, D_0 can be deduced. From D_0, in turn, the hydrodynamic particle radius,

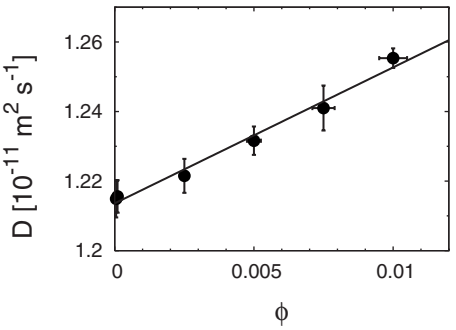

FIG. 1. Measured collective diffusion coefficient, D, obtained by DLS as a function of the silica particle volume fraction, ϕ, for a salt concentration of $c_s=0.15$ mol/l.

R_0, is determined using the Stokes–Einstein relation $D_0=k_BT/(6\pi\eta_0R_0)$. The solvent viscosity, η_0, of water at $T=295.15$ K is taken from the literature as $\eta_0=0.959$ mPa s.[39]

In Fig. 1, the measured collective diffusion coefficient of nonaggregated silica spheres is plotted for samples of varying volume fractions, ϕ, determined by a low-ϕ extrapolation. The line represents a fit to the expression

$$D(\phi)=D_0(1+k_d\phi), \tag{20}$$

which is the low-density form of the collective diffusion coefficient, $D(\phi)$, applicable for a sufficiently large value κa.[40] For $\phi=0$, the single-particle coefficient D_0 is recovered. From our fits, we have obtained $D_0=(1.214\pm0.001)\times10^{-11}$ m^2 s^{-1}. Using the single-particle Stokes–Einstein relation, the hydrodynamic radius of the silica particles is obtained as $R_0=(18.6\pm0.1)$ nm. For the first virial coefficient, we find $k_d=3.2\pm0.2$. Without HIs,

$$k_d=-24\phi\int_0^\infty dx x^2(\exp[-\beta u(x)]-1), \tag{21}$$

where $x=r/(2a)$. Since the negative-valued HI correction to k_d is quite small for the large salt content considered here,[40–42] a positive value of k_d indicates that $u(r)$ is practically repulsive. For a hard-sphere dispersion, a smaller coefficient, $k_d=1.454$,[40] is obtained as in the system considered here. A transmission-electron-microscope (TEM) picture of silica particles is shown in Fig. 2(a), and the histogrammatic size distribution in Fig. 2(b). From this histogram, we deduce the mean particle radius $\langle a\rangle=(12\pm2)$ nm, the standard deviation $\sigma=4.4$ nm, and the z-averaged particle radius,

$$\langle a\rangle_z=\frac{\Sigma_i a_i^6 p(a_i)}{\Sigma_i a_i^5 p(a_i)}, \tag{22}$$

of value $\langle a\rangle_z=(14\pm2)$ nm. Here, $p(a_i)$ is the statistical weight for particles of bin radius a_i and the sum extends over all equally spanned bins. The value for $\langle a\rangle_z$ is slightly smaller than the hydrodynamic radius, $R_0=(18.6\pm0.1)$ nm, obtained by DLS. It is common to find quite different values for the mean radius by TEM and DLS.[43–45] The Ludox particles are made of amorphous silica material so that they may shrink when the suspension is dried to make TEM pictures. In principle, our measurements could be influenced also by electrokinetic effects. However, κa in our samples is typically much larger than 1 so that electrokinetic effects arising from the dynamics of electric double layers are expected to be small. In the following, we use the mean radius obtained by TEM in all our model calculations. Note that for notational simplicity, we will denote the mean colloidal sphere radius $\langle a\rangle$ by a in the following. For the employed $M=4\times10^4$, 5×10^5, and 2×10^6 g/mol, the polymer-to-colloid size ratio is $q=0.49\pm0.03$, 1.4 ± 0.1, and 2.6 ± 0.2, respectively.

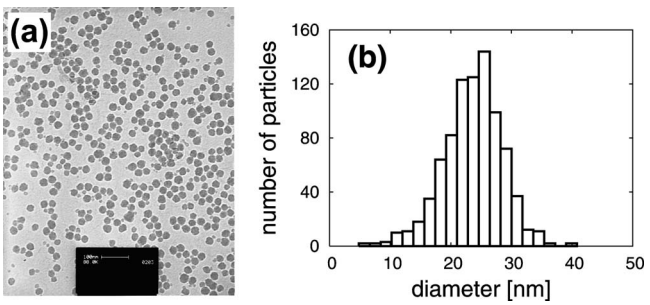

FIG. 2. (a) TEM picture of a dried Ludox particles dispersion. (b) Size distribution of Ludox particles observed from image analysis. The mean particle radius is $\langle a\rangle=(12\pm2)$ nm (see text for details).

Right after sample preparation, an angular-dependent DLS measurement was made for each sample. The so-obtained initial diffusion coefficient, $D(t=0)$, of silica particles which have not yet aggregated was then used as a normalization factor in all subsequent time-dependent DLS measurements. All measurements were made for a fixed scattering angle of $\theta=60°$.

In nondilute samples, we use the single-particle Stokes–Einstein relation, $D(t)=k_BT/(6\pi\eta_0R(t))$, to determine an effective (for $\phi>0$ or $t>0$) hydrodynamic radius, R, from the experimentally observed effective collective diffusion coefficient. The so-obtained effective value of $R(t)$ should be interpreted as an effective hydrodynamic radius[46] deduced from an effective collective diffusion coefficient, $D(t)$, of a nonequilibrium system, which in an average way includes the influence of the (growing) cluster size, an average over the cluster orientations, and also cluster-cluster correlation effects. All samples examined by the DLS measurements were transparent right after mixing. With increasing reaction time, the samples became slightly turbid, indicating the formation of larger clusters or gelation. However, in the present work we focus on the initial stage of aggregation (dimerization), where the samples at low ϕ are transparent and multiple scattering can be safely neglected. From separate measurements of the scattered intensity of a pure polymer solution ($c/c^*=0.84$, $M=5\times10^5$ mol/l) and a pure colloid suspension ($\phi=0.01$), we find that the polymers contribute less than 2% to the total scattered intensity in the colloid-polymer mixture. Thus, the polymer scattering contribution is neglected in our data evaluation.

2. Viscosity of the polymer solution

To account for the increase in the effective viscosity of the colloid dispersion with increasing polymer concentration, the shear viscosity, η, of pure Dextran solutions has been

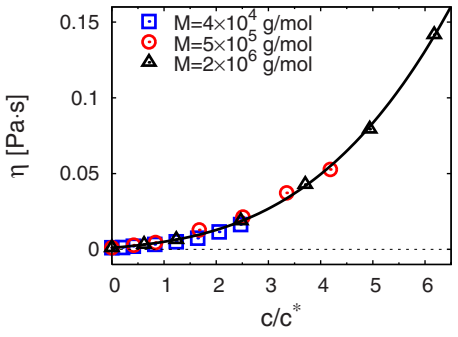

FIG. 3. (Color online) Shear viscosity of a pure dextran solution as a function of the reduced concentration of polymer coils, c/c^*, for three different molecular weights (see legend) at $T=295$ K. The solid curve is a fit to the experimental data (see text).

measured using an Ares 4LS1 rheometer (TA Instruments, USA) with a Couette cell of 17 mm inner diameter. The polymer was diluted in the pure buffer solution without salt. In Fig. 3, the measured viscosity of the dextran solution is shown as a function of the reduced density of polymer coils, for molar masses of $M=4\times10^4$, 5×10^5, and 2×10^6 g/mol, respectively. As expected, η is a function of $y=c/c^*$ only, independent of the molar mass. The solid curve is a fit to the cubic expansion,[47]

$$\eta(y) = \eta_0(1 + \alpha_1 y + \alpha_2 y^2 + \alpha_3 y^3), \tag{23}$$

with $\alpha_1=3\pm1$, $\alpha_2=0.7\pm0.6$, and $\alpha_3=0.43\pm0.07$. The experimentally observed viscosity of the pure buffer solution, $\eta(y=0)=(1.0\pm0.2)\times10^{-3}$ Pa s, is in good agreement with this value. A NaCl concentration of 0.5 mol/l increases the (pure) solvent viscosity only slightly to $(1.1\pm0.2)\times10^{-3}$ Pa s. This small increase is neglected in the following analysis.

3. Evidence that dextran does not adsorb at the silica-water interface

To investigate whether dextran adsorbs at the silica sphere surfaces, we prepared a dispersion of Ludox silica particles and mixed it with dextran solutions of varying concentration. The samples were mixed thoroughly and stored for 24 h at room temperature to allow them to equilibrate before the measurements were conducted. All samples contain an ammonium-chloride buffer of concentration $c_b=0.02$ mol/l and $p\mathrm{H}=9.2\pm0.1$. The volume fraction of Ludox was fixed to $\phi=0.005$. Figure 4 displays DLS measurements on the Ludox-dextran mixtures at varying salt concentrations. As shown, the collective diffusion coefficient, D, and, likewise, the hydrodynamic radius, R, are not affected upon increasing the polymer concentration. If the polymers would adsorb, one would expect instead a significant decrease of D and, conversely, an increase in R due to the enlarged hydrodynamic friction caused by adhering chains. Thus, we conclude that dextran does not adsorb on the Ludox particles at $p\mathrm{H}=9.2\pm0.1$, in agreement with previous findings for silica spheres.[49–51]

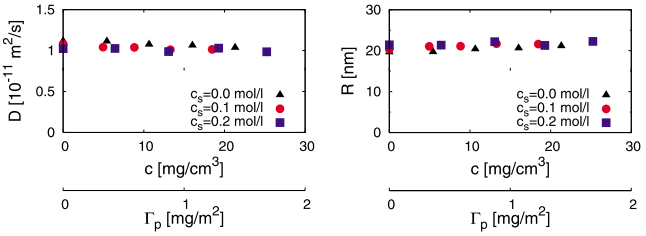

FIG. 4. (Color online) Left: Collective diffusion coefficient, D, of a Ludox silica dispersion at $\phi=5\times10^{-3}$ as a function of added dextran concentration, c, ($M=5\times10^5$ g/mol), for $c_s=0$, 0.1, and 0.2 mol/l, respectively. Right: Effective hydrodynamic radius, R, obtained from the single-particle Stokes–Einstein relation using $\eta_0=0.959$ mPa s. The lower scale of the abscissa gives the polymer surface concentration, Γ_p, that would result if all polymers did adsorb on the surface of the silica particles. As a rule of thumb, the surface is completely covered when $\Gamma_p\geq1$ mg/m^2 (Ref. 48).

IV. RESULTS AND DISCUSSION

A. Cluster-aggregation in pure silica dispersions

We first explore aqueous suspensions of silica particles without added polymers. Earlier studies used colloidal batches different from ours in terms of the particle size and densities, and with different solvent conditions.[52–57] Our light scattering data on the pure silica-water system discussed in the following serve as the basis to study the additional influence of added polymers on the cluster aggregation rate.

B. Effect of the salt concentration on the aggregation rate

In Fig. 5, the time-resolved effective collective diffusion coefficient, $D(t)$, of a polymer-free silica sphere dispersion at $\phi=0.01$ and $p\mathrm{H}=9.2$, was measured over several hours and for various salt concentrations c_s. The plotted diffusion coefficient is normalized by the single-particle diffusion coefficient D_0. As can be seen, the time evolution of $D(t)$ depends strongly on c_s. With increasing c_s, D decays faster to zero, which is indicative of a more quickly growing cluster size of aggregates. This observation is explained by the salt-induced screening of the colloid charges. The electrostatic repulsion decreases with increasing c_s so that the particles can overcome the reduced Coulomb barrier more easily during a collision event, leading to the formation of dimers, trimers, and so on. With growing reaction time, increasingly larger aggregates are observed, consisting of several silica particles (monomers). As a consequence, the effective diffusion coef-

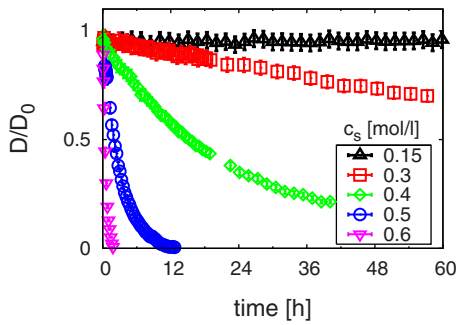

FIG. 5. (Color online) Normalized measured time-dependent (effective) collective diffusion coefficient of Ludox spheres as a function of the elapsed time after sample preparation, for varying c_s (see legend) and $\phi=0.01$.

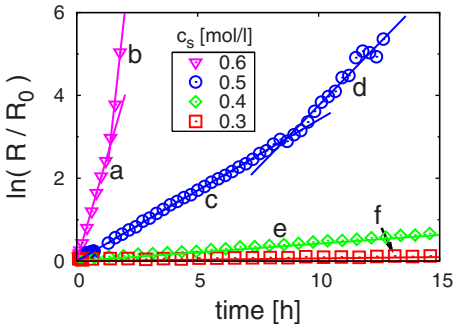

FIG. 6. (Color online) Semilogarithmic plot of the reduced time-dependent effective hydrodynamic radius of colloid clusters deduced for several salt concentrations as a function of time for $\phi=0.01$. The straight line segments are fits to the form $R(t)=R_0\exp(t/\tau_a)$, with the aggregation time τ_a. $c_s=0.6$ mol/l (▽): (a) $\tau_a=(0.498\pm0.003)$h, (b) $\tau_a=(0.19\pm0.02)$h; $c_s=0.5$ mol/l (○): (c) $\tau_a=(2.93\pm0.01)$h, (d) $\tau_a=(1.67\pm0.07)$h; $c_s=0.4$ mol/l (◇): (e) $\tau_a=(23.8\pm0.1)$h; $c_s=0.3$ mol/l (□): (f) $\tau_a=(7.8\pm0.1)$d, respectively.

ficient of the colloid aggregates decreases, and likewise, the effective cluster hydrodynamic radius, R, increases with time.

In Fig. 6, the logarithm of the reduced effective hydrodynamic radius is plotted as a function of the time elapsed after sample preparation, for a series of samples with $c_s\geq0.3$ mol/l. For all salt concentrations considered, a linear relation for initial times is observed within the logarithmic-linear plot. From this, we conclude that the initial cluster growth of the charged colloids is caused by an irreversible reaction-limited aggregation (RLA) process, for which the effective hydrodynamic radius scales in time as $R\sim\exp(t/\tau_a)$. For $c_s=0.5$ and 0.6 mol/l, a second and faster developing exponential cluster growth regime is observed at later times. This regime can be attributed to a faster irreversible reaction-limited cluster aggregation mechanism, which sets in once the clusters have consumed most of the monomers in their surroundings.

The initial aggregation time, τ_a, deduced in Fig. 6 from the linear fit to the short-time data points, is shown in Fig. 7 as a function of c_s. It can be noticed that τ_a depends sensitively on c_s. Increasing c_s from 0.15 to 0.6 mol/l, reduces τ_a from several weeks down to half an hour. Note here that the τ_a depicted for $c_s=0.15$ mol/l has been monitored by angular-dependent DLS over a period of 16 days.

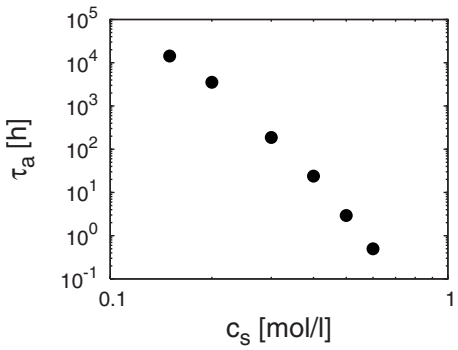

FIG. 7. Initial aggregation time, τ_a, as a function of salt concentration c_s, for $\phi=0.01$.

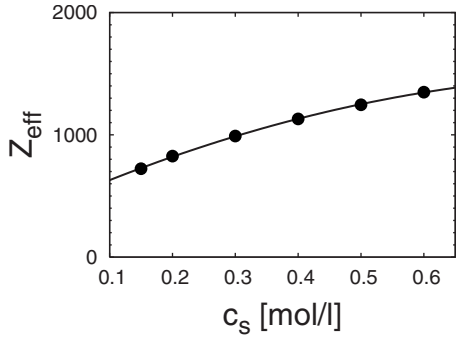

FIG. 8. Effective colloid charge number as a function of added salt concentration, obtained from matching Eq. (5) to the experimentally determined initial aggregation time τ_a given in Fig. 7. The solid curve is a fit to the form $Z_{\rm eff}(c_s)=b_1c_s^2+b_2c_s+b_3$, with $b_1=(-1184\pm90)$ $l^2/{\rm mol}^2$, $b_2=(2267\pm68)$ l/mol, and $b_3=413\pm12$.

C. Theoretical description of the aggregation rate

The initial aggregation process can be described by the dimer formation theory introduced in Sec. II A and outlined in Appendix. A polymer-free dispersion of silica particles is described by substituting $u(r)\equiv u_{\rm DLVO}(r)$ in Eq. (6), using a Hamaker constant of $A_H=0.8\times10^{-20}$ J.[58] The only unknown parameter in $u_{\rm DLVO}(r)$ is the effective charge number. For consistency, we have determined $Z_{\rm eff}$ in Eqs. (2) and (3) by matching τ_a, calculated according to Eq. (5), to the experimental values given in Fig. 7. Since the major contribution to the integral in Eq. (6) stems from the vicinity of the maximum in $u(r)$, we can use a lower cutoff radius $a+\epsilon$. Values of ϵ in between 0.1 and 0.2 nm have been employed.[26] In the present system of highly screened nanosized particles, the maximum in $u_{\rm DLVO}(r)$ occurs at subnanometer distances. Hence, for $a+\epsilon$, we selected the radial distance r_0, where $u_{\rm DLVO}(r)$ crosses zero close to contact. The effective charge number, $Z_{\rm eff}$, obtained by this matching procedure is plotted in Fig. 8 as a function of c_s. In Fig. 9, the corresponding pair potential is presented. The increase in $Z_{\rm eff}$ with increasing c_s conforms to the lowering of counterion condensation caused by enlarged screening.[59] Table I contains the numerical values characterizing the pair potential. The location of the maximum (Coulomb barrier), $r_{\rm max}$, and the secondary minimum, $r_{\rm min}$, in $\beta u_{\rm DLVO}$ range from $r_{\rm max}/(2a)=1.007$ to 1.006, and from $r_{\rm min}/(2a)=1.26$ to 1.10, respectively, when c_s is

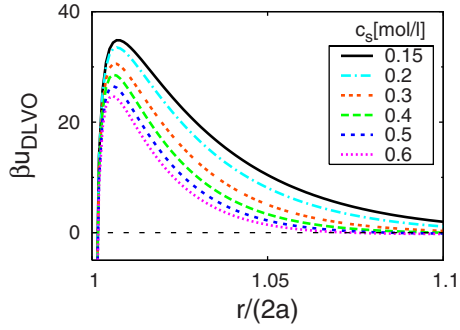

FIG. 9. (Color online) DLVO pair potential for parameters obtained from adjusting the effective colloid charge number $Z_{\rm eff}(c_s)$, entering the calculation of τ_a, to the experimentally found initial aggregation time, for a system with $\phi=0.01$ at $T=295$ K (see Table I).

TABLE I. Parameters characterizing $u_{\mathrm{DLVO}}(r)$ for several experimentally analyzed salt concentrations. The effective charge number, Z_{eff}, has been adjusted to obtain the experimental values of τ_a without added polymers as described in the text.

c_s (mol/l)	Z_{eff}	$1/(\kappa\sigma)$	$\beta\epsilon$	Q (k_BT)	τ_a (h)
0.15	723	0.032	56.6	34.9	14 329
0.2	826	0.028	56.8	33.6	3533
0.3	990	0.023	55.9	30.7	186
0.4	1130	0.020	55.6	28.7	24
0.5	1246	0.018	54.6	26.7	2.9
0.6	1349	0.016	53.8	25.0	0.5

increased from 0.15 to 0.6 mol/l. Likewise, the reduced pair potential at $r_{\max}$, $\beta u_{\mathrm{DLVO}}(r_{\max})$, decreases from 35 to 25, and the depth of the secondary minimum, $\beta u_{\mathrm{DLVO}}(x_{\min})$, deepens from -0.04 to -0.24. The radial distance, r_0, where u_{DLVO} crosses zero near contact, is almost unaffected by the salinity changes, with a nearly constant value of $r_0=1.002$, whereas the Coulomb barrier height, Q, is strongly affected. See Table I for a summary of these parameters.

For values $l_B|Z|/a \gtrsim 1$, where Z is the bare colloidal charge number, the linear Debye–Hückel (DH) assumption underlying Eq. (2) does not apply any more. In fact, we have $l_B|Z|/a > 50$ in our silica dispersions, for all c_s considered. For large colloid charges, the DH form of $u_{\mathrm{el}}(r)$ can still be used, but Z and also κ must be replaced by an effective (renormalized) charge number Z_{eff}, and a renormalized κ, that incorporate the effect of quasicounterion condensation at strongly charged colloid surfaces. Due to this counterion condensation effect, Z_{eff} can be substantially smaller than the bare charge, in particular, at lower salinity. Similar charge renormalization problems have been encountered before in experimental studies on dispersions of highly charged submicron silica particles without polymers.[60]

The relative interparticle distance $r-2a$, where the maximum in $u_{\mathrm{DLVO}}(r)$ occurs, is in the subnanometer range for the small Ludox particles and the high salt concentrations considered. Thus, the continuum description of the solvent underlying the Poisson–Boltzmann theory cannot be fully justified any more, and the discrete nature of microions and solvent molecules may play a role. Also, the form of the vdW attraction may not be quantitatively describable any more by Eq. (1), and particle surface roughness effects,[61,62] inhomogeneous surface charge distribution,[63,64] and hydration forces[65,66] should also be considered in principle. A quantitative model including all these additional features would be extremely demanding and has not been worked out to date. Since our present work focuses on the essential features of the influence of polymer-induced attraction on the nonequilibrium and equilibrium phase behavior of charge-stabilized nanometric colloidal dispersions, we are not concerned here with such a first-principle description. Instead, we restrict ourselves to the DLVO-type description and consider the value of Z_{eff} in $u_{\mathrm{el}}(r)$ as an adjustable parameter, from which the renormalized κ of a 1-1 electrolyte is determined by Eq. (3) with Z replaced by Z_{eff}, in accord with the renormalized jellium model of charge renormalization.[59]

For later discussion, we point out that $Z_{\mathrm{eff}}(c_s)$ is determined from matching the calculated τ_a to the experimental one using a selected value $\phi=0.01$. This value of $Z_{\mathrm{eff}}(c_s)$ is assumed to be constant when ϕ is changed to other values.

D. Influence of colloid volume fraction on aggregation rate

We investigate here the influence of the colloid volume fraction varied in the range from 0.01 to 0.14, for two different salt concentrations of $c_s=0.15$ and 0.3 mol/l, respectively. The measured initial collective diffusion coefficient at $t=0$ increases with increasing ϕ and decreasing c_s, corresponding to values $k_d>0$ [see Eqs. (20) and (21)], akin to what is observed for the collective diffusion coefficient in stable charge-stabilized suspensions.[40] Indeed, the DLS deduced values $D(t=0)=(1.258\pm0.005)\times10^{-11}$ m^2 s^{-1} at $c_s=0.3$ mol/l and $\phi=0.12$, and $D(t=0)=(1.434\pm0.002)\times10^{-11}$ m^2 s^{-1} at $c_s=0.15$ mol/l and $\phi=0.12$, are all larger than $D_0=(1.214\pm0.001)\times10^{-11}$ m^2 s^{-1}, the latter measured at $c_s=0.15$ mol/l. As for stable suspensions, we attribute this to the influence of particle correlations since, at $t=0$, aggregation has not been set in significantly.

In Fig. 10, the (effective) hydrodynamic radius deduced from the collective diffusion coefficient measured at a nondiluted sample is plotted as a function of time for samples with $c_s=0.15$ and 0.3 mol/l and various ϕ, showing that the colloid cluster growth is enhanced with increasing ϕ and c_s.

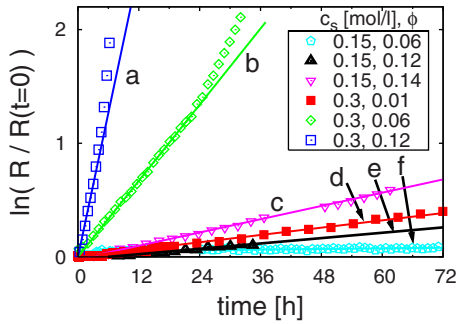

FIG. 10. (Color online) Semilogarithmic plot of the effective hydrodynamic radius of aggregated colloidal clusters as a function of the elapsed time. The straight lines (a)–(f) are fits to the form $R(t)=R(t=0)\exp(t/\tau_a)$, with the parameters τ_a and $R(t=0)$ determined right after the sample preparation. The data for $\phi=0.01$, and $c_s=0.3$ mol/l are replotted for comparison from Fig. 6. $c_s=0.15$ mol/l: (⌂, f) $\phi=0.06$, $\tau_a=(94\pm9)$d; (▲, e) $\phi=0.12$, $\tau_a=(10.6\pm0.2)$d; (▽, c) $\phi=0.14$, $\tau_a=(4.29\pm0.02)$d; $c_s=0.3$ mol/l: (■, d) $\phi=0.01$, $\tau_a=(7.8\pm0.1)$d; (◇, b) $\phi=0.06$, $\tau_a=(17.9\pm0.1)$h; (□, a) $\phi=0.12$, $\tau_a=(4.7\pm0.2)$h.

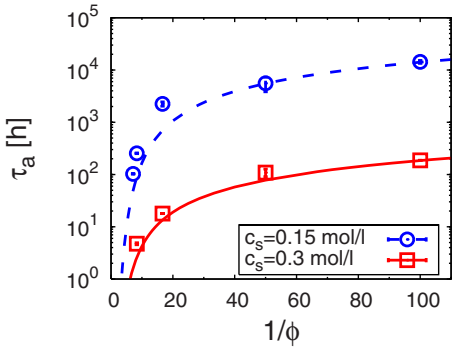

FIG. 11. (Color online) Aggregation time, τ_a, as a function of inverse colloid volume fraction, for c_s=0.15 mol/l (○) and c_s=0.3 mol/l (□). The dashed and solid curves are the theoretically predicted aggregation times for c_s=0.15 mol/l and 0.3 mol/l, respectively, calculated from Eq. (5), using $u_{\mathrm{DLVO}}(r)$ in Eq. (4) (see also Fig. 9).

A significant influence of ϕ on τ_a can be expected from the fact that the collision probability increases with ϕ. The logarithm of the normalized hydrodynamic radius (see Fig. 10) follows a linear time relation for short times after sample preparation, indicating a slow RLA mechanism. However, for c_s=0.3 mol/l and $\phi \geq 0.06$ and later times, we find a nonexponential cluster growth. This nonexponential growth rate can be attributed to the gelation of the sample, which manifests itself in a power-law-dependent growth rate.[67] Consistent with our expectation of a growth rate that increases with ϕ, τ_a deduced from the data points in Fig. 10 increases with increasing $1/\phi$ indeed (see Fig. 11). Also shown in Fig. 11 is the theoretically predicted aggregation time, calculated from Eq. (5) using values for Z_{eff} given in Fig. 8. The dimer formation theory of the initial stage of Brownian flocculation describes our experimental data quite well, for volume fractions $\phi \leq 0.14$. In more concentrated colloidal suspensions not considered in this work, we expect an enhanced aggregation rate arising from the reduced volume available to the microions caused by the macroionic excluded volumes,[68,69] and from intercolloid correlation effects observed by Sauer and Löwen[70] in their computer simulations. In addition, the influence of the microion finite sizes on their screening abilities, and additional electrostatic screening caused by intervening macroions, may play a role at high colloid concentrations.[71]

E. Effect of added nonadsorbing polymer chains

So far, we have considered polymer-free silica dispersions only. In the following, we analyze the influence of the depletion agent dextran on the aggregation kinetics. On adding dextran polymers of molar mass $M=5\times10^5$ g/mol ($q=1.4\pm0.1$) to a charge-stabilized dispersion at ϕ=0.01 and c_s=0.15 mol/l, no enhanced creation of clusters is observed even up to $c/c^*=1.67$, and for an observation time extending over two days after sample preparation. This indicates that at c_s=0.15 mol/l, the polymer-induced depletion attraction is not strong enough to change the aggregation behavior significantly.

However, for a larger c_s=0.3 mol/l we do observe a strong influence of c_s on the aggregation behavior. Plotting $R(t)$ versus the observation time on a logarithmic-linear

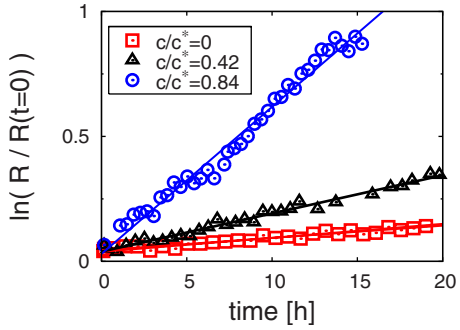

FIG. 12. (Color online) Semilogarithmic plot of the reduced effective hydrodynamic radius of colloid clusters as a function of elapsed time, for a mixture of Ludox silica spheres at ϕ=0.01 and dextran at varying concentrations, with $q=1.4\pm0.1$, and c_s=0.3 mol/l. The straight lines are fits to the form $R(t)=R(t=0)\exp(t/\tau_a)$, with the characteristic time τ_a and the effective hydrodynamic radius $R(t=0)$ measured right after sample preparation. For comparison, the data points for $c/c^*=0$ are replotted from Fig. 6. $c/c^*=0$: (□)$\tau_a=(7.8\pm0.1)$d; $c/c^*=0.42$: (△) $\tau_a=(2.7\pm0.1)$d; $c/c^*=0.84$: (○) $\tau_a=(16.2\pm0.1)$h.

scale, results in a linear relation (see Fig. 12), and now the clusters grow faster with increasing c/c^*. This observation is in accordance with previous findings.[24] It suggests that the addition of nonadsorbing polymers at near-θ solvent conditions does not change the aggregation mechanism. Hence, also in the presence of polymer chains, the initial cluster growth is likely to be determined by the RLA mechanism. The values of τ_a depicted in Fig. 13 have been determined from the slopes to the curves in Fig. 12. Decreasing values of τ_a with increasing c correspond to an enhanced cluster growth rate. The dotted magenta curve in Fig. 13 is our theoretical prediction for $\tau_a(c)$, obtained using Eqs. (5) and (6), and the DLVO potential in conjunction with the AOV potential. Note again here that Z_{eff} was determined from matching the experimental τ_a for systems without added polymers. Thus, no adjustable parameter is added in the presence of polymers. As shown in Fig. 13, the effect on τ_a due to added polymer chains is overall well described by the AOV potential. The aggregation times predicted by the initial aggregation theory are moderately larger than the corresponding experimental values, with increasing differences for increasing c/c^*.

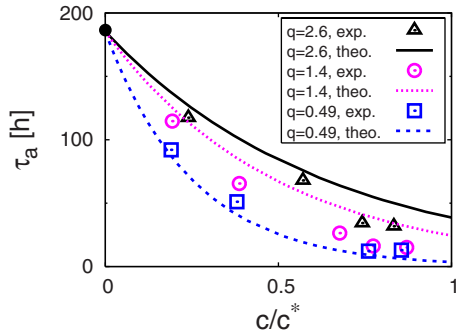

FIG. 13. (Color online) The data points (symbols) give the experimentally determined aggregation time as a function of the reduced polymer concentration, in a mixture of dextran with varying range of attractions, $q=0.49\pm0.03$ ($M=4\times10^4$ g/mol), $q=1.4\pm0.1$ ($M=5\times10^5$ g/mol), and $q=2.6\pm0.2$ ($M=2\times10^6$ g/mol), respectively, and silica particles with $\phi=0.01$ and c_s=0.3 mol/l. The curves are the theoretically predicted τ_a based on the AOV potential and values of Z_{eff} as explained in Sec. II B.

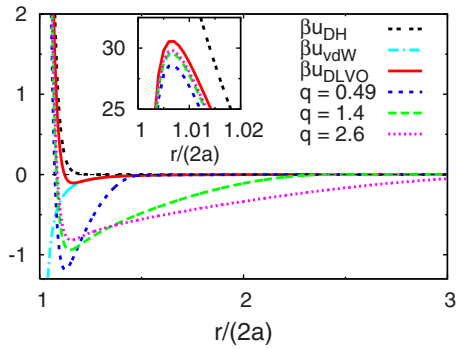

FIG. 14. (Color online) Total pair potential for $q=0.49\pm0.03$ ($M=4\times10^4$ g/mol), $q=1.4\pm0.1$ ($M=5\times10^5$ g/mol), and $q=2.6\pm0.2$ ($M=2\times10^6$ g/mol), with $\phi=0.01$, $c_s=0.3$ mol/l, $c_b=0.01$ mol/l, $T=295$ K, and fixed polymer concentration, $c/c^*=0.5$. The black dashed curve is the repulsive electrostatic part, and the dashed-dotted (turquoise) curve the short-ranged vdW part of $u(r)$. The inset displays the Coulomb barrier part of $u(r)$ located at smaller particle separations.

F. Effect of polymer-to-colloid size ratio *q* on the aggregation rate

In Fig. 13, we show τ_a in dependence on the polymer concentration for samples of varying molar mass corresponding to $q=0.49-2.6$, at fixed $c_s=0.3$ mol/l and $\phi=0.01$. We find here a τ_a that decreases with increasing c/c^* for all q values considered. Moreover τ_a becomes larger for larger q. A similar behavior has been reported by Seebergh and Berg[24] for $q\leq0.21$. The curves in Fig. 13 are our theoretical results for $\tau_a(c)$. Considering the approximations entering the dimer formation theory, the overall agreement between experiment and theory is quite good. For $q=0.49$, the data points are located above the theoretical curves, whereas the experimental values are overestimated for $q=1.4$ and 2.6. The deviations increase with increasing c/c^*. For all q-values and polymer concentration investigated in our work, we observe an exponential cluster growth rate indicative of a RLA process.

The findings discussed above can be explained as follows: $1/\tau_a$ grows with increasing c due to the increasing osmotic pressure, which drives the colloidal particles together, and thus promotes colloidal aggregation. In Fig. 14, the various potential contributions to the total $u(r)$ are plotted for $q=0.49$, 1.4, and 2.6, respectively, and for a fixed $c/c^*=0.5$ and $c_s=0.3$ mol/l. The comparison of the full potential form of $u(r)$ at varying q with $u_{\mathrm{DLVO}}(r)$ reveals that the polymer depletion effect described by $u_{\mathrm{AOV}}(r)$ adds a longer-ranged attractive part to $u(r)$. Thus, polymer-induced depletion reduces the height of the Coulomb barrier, and creates a pronounced secondary minimum with a depth of about $1k_BT$. As a consequence, τ_a decreases with increasing c/c^*, and so does the stability ratio W defined in Eq. (6). At fixed c/c^*, the strength of the AOV depletion attraction decreases for increasing q [see Eq. (7)], whereas the range of attraction is growing with q. Thus, the effect of the increasing depletion range is outweighted by its decreasing strength (see here Fig. 14). Accordingly, W and τ_a both increase with increasing q for fixed c/c^*, giving rise to a slower growth of clusters. The experimentally observed τ_a decreases faster with increasing c than the theoretical prediction for $q>1$ and $c/c^*\gtrsim0.8$. This can be explained by the nonideal solution behavior of dextran, which is not accounted for in the AOV model. As shown in Fig. 4 of Ref. 16, where the influence of polymer nonideality is considered, the thickness of the depletion layer starts to decrease quickly for increasing polymer concentrations near c^*, and for $q>1$, since the colloid size is then comparable to the polymer correlation length. Therefore, the range of the polymer-induced colloid attraction shrinks with increasing c/c^*. In addition, the osmotic pressure exerted by the polymers on the colloids increases rapidly (for $q>1$) with increasing c/c^* (see again Fig. 4 in Ref. 16) so that the strength of the depletion attraction increases. Both effects, the decrease in range and the increase in strength of the depletion attraction, enhance the formation of clusters as observed in our experiments.

G. Nonequilibrium state diagrams

The silica-dextran mixtures investigated so far were characterized by a low $\phi=0.01$ and low polymer concentrations $c\lesssim c^*$. These samples initially form a homogeneous and transparent mixture. With progressing time, the samples gradually turn turbid. On the basis of our measurements of $R(t)$ and τ_a discussed before, we attribute the increasing sample turbidity to the growth of colloidal clusters (for samples with $\phi=0.01$). If these samples are without added polymers, they form a space-spanning solid gel at later times. When polymer chains are added, the cluster aggregation process is accelerated (recall here Secs. IV E and IV F).

The dispersions behave quite differently when ϕ and c are increased at low salt content (i.e., for $0.1\leq c_s\leq0.2$ mol/l). At high ϕ and c, and low c_s, the samples become turbid right after mixing. Several hours or days later, depending on the actual colloid, polymer and salt concentrations, a turbid and highly viscous fluidlike phase can form at the container bottom. On top of this viscous bottom phase, a slightly turbid fluidlike phase is observed. A sharp interface between the two fluidlike phases is visible. We point out that these are two nonequilibrium fluidlike phases. With increasing observation time, the bottom phase ceases to flow, and forms a white gel-like phase after several days up to a few

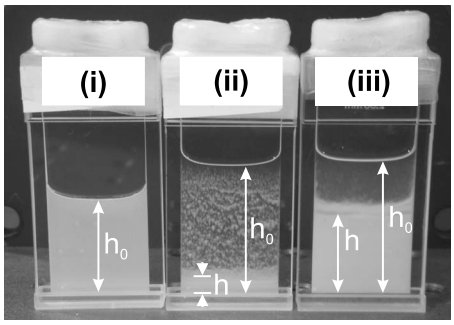

FIG. 15. Photographs of samples containing a colloid-polymer mixture with $c_s=0.15$ mol/l [see also Fig. 16(c)], and polymer molar mass $M=5\times10^5$ g/mol. The picture has been taken two days after sample preparation. Sample (i) with $\phi=0.04$ and $c/c^*=2.93$ has become turbid and forms a gel at later times. In sample (ii), where $\phi=0.09$ and $c/c^*=1.26$, and sample (iii), where $\phi=0.09$ and $c/c^*=2.09$, two phases are observed. The total height, h_0, of the dispersion and the height, h, of the more turbid bottom phase are indicated by arrows.

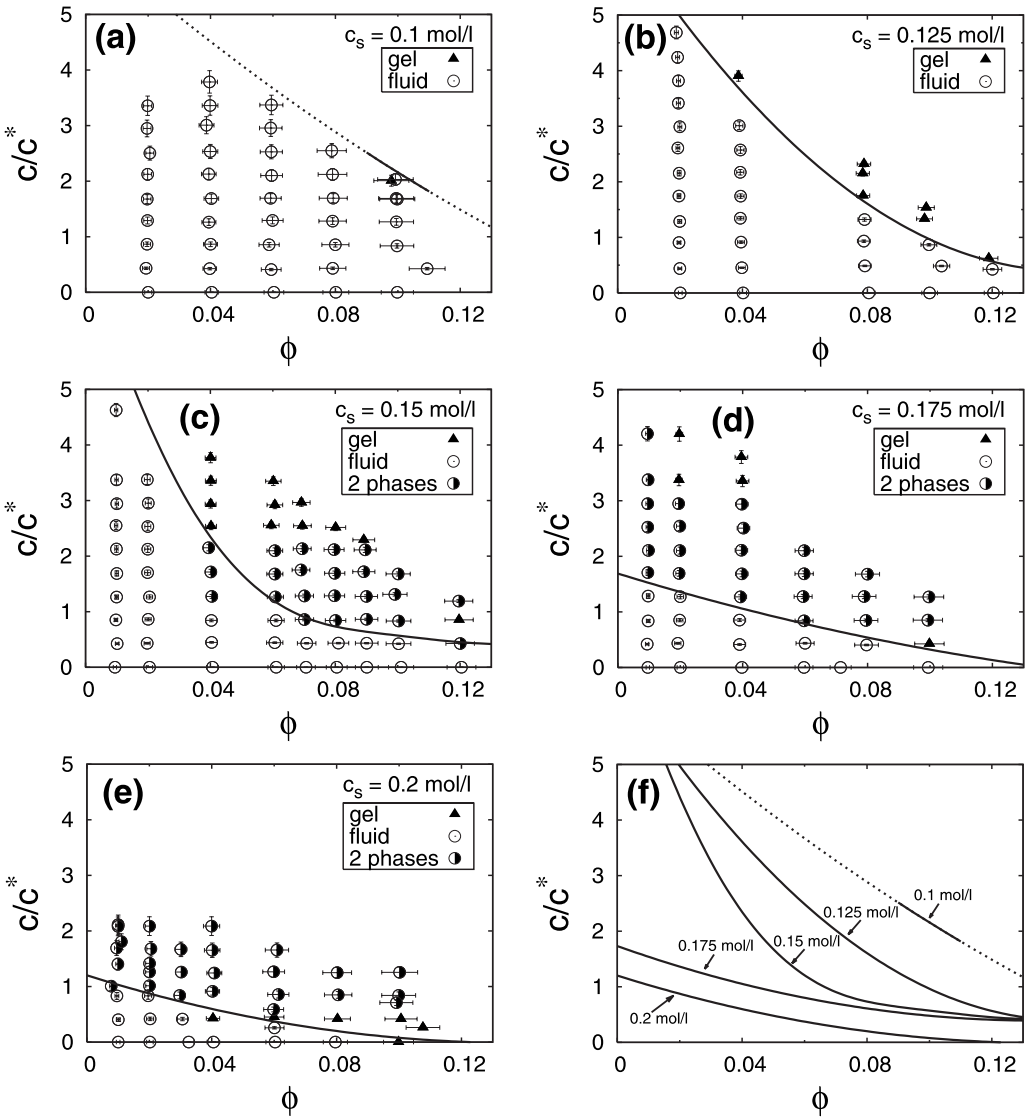

FIG. 16. Nonequilibrium state diagrams of aqueous mixtures of Ludox silica particles and dextran for varying salt concentrations: [chart (a)] c_s =0.1 mol/l, (b) c_s=0.125 mol/l, (c) c_s=0.15 mol/l, (d) c_s=0.175 mol/l, and (e) c_s=0.2 mol/l for $q=(1.4\pm0.1)$ nm ($M=5\times10^5$ g/mol) at room temperature. The phase diagrams of the samples have been recorded by visual inspection two weeks after sample preparation. Open circles (○) indicate fluidlike homogeneous mixtures. The half-filled circles (◑) describe samples, where a turbid viscous phase is observed at the container bottom. The triangles (▲) mark samples that form a gel throughout the sample. The solid dividing curves are guides to the eye, separating the single-fluid phase region from the region where phase separation or a system-spanning gel is observed after 2 weeks. For all salt concentration considered, these dividing curves are summarized in (f).

weeks. During the same time span, the upper fluidlike phase gradually becomes transparent (see Fig. 15). The time until this macroscopic phase separation occurs, and the time until the bottom phase forms a gel depend on c, c_s, and ϕ. This dependence has not been studied systematically in the present work. The investigation of the (time-dependent) microstructure and rheology of the bottom phase is left to future studies.

For c_s in the range of 0.1 and 0.2 mol/l, the nonequilibrium state diagram obtained 2 weeks after sample mixing by visual inspection is shown in Fig. 16. The dividing curves are just guides to the eye to distinguish systems in a slightly turbid but homogeneous single phase (○) from samples which have phase separated (◑), as already described above, or have formed a system-spanning gel (▲), without undergoing a (macroscopic) demixing process. For the c_s =0.1 mol/l systems in Fig. 16(a), the colloid-polymer mixture has not phase separated for all considered colloid and polymer concentrations even 2 weeks after sample mixing. Only the sample with ϕ=0.1, c/c^*=2.09, and c_s =0.1 mol/l has formed a gel. On increasing c_s to 0.125 mol/l [see Fig. 16(b)], the samples either form a gel at high c and ϕ, or stay mixed, without phase separation within the two weeks of observation time. However, for c_s=0.15 and 0.175 mol/l [see Figs. 16(c) and 16(d), respectively] and after 2 weeks, we observe a homogeneous fluidlike sample for low c/c^* and ϕ, phase separated samples for intermediate polymer and colloid concentrations, and gelated samples at high c/c^*. For an even higher salt concentration of c_s =0.2 mol/l [Fig. 16(e)], we unexpectedly observe that sample-spanning gels appear at lower c/c^*-values than those of the phase separating samples. According to Fig. 16, the dividing curve moves to lower ϕ and smaller c with increas-

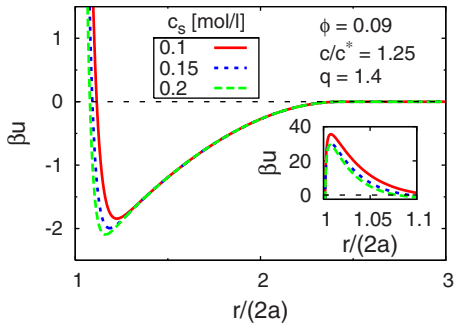

FIG. 17. (Color online) Reduced total pair potential, $\beta u(r)$, for c_s=0.1, 0.15, and 0.2 mol/l with ϕ=0.09, c/c^*=1.25, and q=1.4 (M=5×10^5 g/mol). The inset shows the Coulomb barrier part.

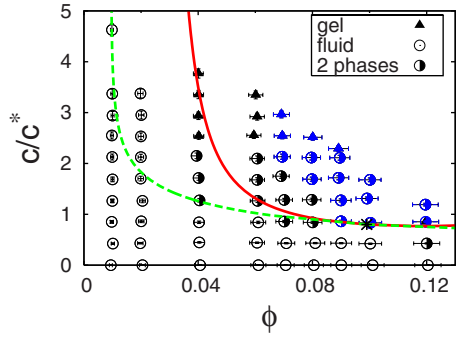

FIG. 18. (Color online) Time evolution of the nonequilibrium state diagram for an aqueous mixture of silica particles and dextran, with c_s=0.15 mol/l and q=(1.4±0.4) nm (M=5×10^5 g/mol). The gray (blue) symbols give the state of the sample two days after sample preparation. The black symbols describe the state after 2 weeks. The theoretically predicted binodal [dashed (green) curve] and spinodal [solid (red) curve] are obtained form GFVT on assuming θ-solvent conditions. The asterisks denote the critical point.

ing c_s. This is most clearly seen in Fig. 16(f). Moreover, the dividing curve shifts to lower ϕ- and c/c^*-values with increasing observation time (see Fig. 18).

In Fig. 17, we plot $u(r)$ for ϕ=0.09, c/c^*=1.25, and varying c_s. Since the Coulomb barrier is lowered with increasing amount of salt (see the inset of Fig. 17), the dividing line in Fig. 16 can be expected to move faster in time to lower ϕ- and c-values with increasing c_s, in accordance with the experimental observations in Fig. 16(f). As revealed by Fig. 17, the polymers induce a long-ranged attraction into a pronounced secondary minimum, which can drive a reversible phase separation. Note here the comparatively high Coulomb barrier depicted in the inset of Fig. 17 which prevents fast aggregation.

Our observation that samples at high ϕ and c turn turbid immediately after mixing, could be an indication of a spinodal decomposition driven by the long-ranged polymer depletion effect. To differentiate between irreversible aggregation and phase separation in the initial state after sample preparation, a control experiment was performed: A test sample was prepared with ϕ=0.09, c/c^*=1.26, M=5×10^5 g/mol, and c_s=0.15 mol/l which turned turbid immediately. A few hours later this sample was diluted by adding a buffer solution of the same c_s. A DLS experiment on the diluted sample gave then an effective hydrodynamic radius R=(21.2±0.4) nm rather close to the colloid radius. This observation indicates that the initial demixing process, causing the turbidity right after sample preparation, is reversible, and indeed might be due to spinodal decomposition or a nucleation and growth process. However, when the original test sample was diluted not a few hours but a few days after its preparation, we found that a colloid gel was formed on the container bottom which could not be redispersed. Thus, the irreversible aggregation proceeds slower than the phase separation (see also Fig. 7).

In the following, we discuss whether, for high ϕ and c, the observed nonequilibrium phase separation and gelation processes are initiated by spinodal decomposition, and how the aggregation process interferes with the faster initial equilibrium phase separation process. Lu *et al.*[8] provided ample evidence that gelation is driven by spinodal decomposition, at least in colloid-polymer mixtures of very short-range depletion attraction (q=0.059). Similar experimental observations were made earlier by Grant and Russel,[72] who studied a dispersion of sterically stabilized silica particles in an organic solvent. Both groups found that the gelation line coincides with the spinodal line at low ϕ. Grant and Russel,[72] in addition, showed for systems without polymers but with vdW attraction that the spinodal line is metastable with respect to the fluid-solid coexistence curve. Notice, however, that Lu *et al.* investigated systems of polymer-grafted colloids, with hard-sphere-like interactions, and with polymer chains of low-molar weight that induce only very short-ranged attractions. In contrast to this, we study here a more complex system of charged colloids with short-ranged vdW and long-ranged polymer depletion attractions. In systems with long-ranged depletion attraction ($q \gtrsim 0.3$), the gel line often extends into the stable gas-liquid coexistence region well below the critical point.[4,12]

Figure 18 shows the binodal and spinodal lines calculated by GFVT for a stable colloid-polymer system at c_s=0.15 mol/l without vdW attractions included. These lines are shown in search of possible relations between the experimental nonequilibrium state diagram 2 days and 2 weeks after sample preparation, which are also shown in the figure, and the GFVT phase behavior prediction. As seen, all samples which phase separate two days after mixing, are located within the GFVT predicted spinodal region located to the right of the solid red spinodal line in Fig. 18. Notice further that the samples which were not phase separated after 2 days but have phase separated after 2 weeks are located in the GFVT metastable region in between the dashed green binodal and the solid red spinodal lines.

We point out that the phase diagram obtained after 2 weeks continues to evolve in time. For example, the sample with ϕ=0.02 and c/c^*=2.09, that was still homogeneous after 2 weeks, is phase separated, and the samples with ϕ=0.02 and $c/c^* \gtrsim 3$ are forming a gel after 3 weeks waiting time. How all the samples develop at even longer times has not been recorded in our study. The observation that all samples which have phase separated after 2 days are located within the thermodynamically unstable region predicted by the GFVT bounded from the left by the solid red spinodal line, does indicate that the experimentally observed phase

separation and gelation processes are initiated on crossing the spinodal line, as observed also by Lu *et al.*[8] We conjecture that the colloids start to aggregate within the denser, colloidal-rich regions during the faster progressing demixing process. Since the colloids are not buoyancy matched, larger clusters should sediment to the container bottom to form the lower turbid phase. Later on, we expect that the sedimented clusters aggregate irreversibly in the bottom phase and form a gel. This two-stage picture is supported by the fact that the dimer formation theory for $\phi=0.09$, $c/c^*=1.25$, and $c_s=0.15$ mol/l gives a value of $\tau_a \approx 18$ h consistent with an irreversible aggregation that is observed experimentally only for delay times of the order of days. Recall, however, that vdW attraction has been neglected in the GFVT equilibrium calculations, and that GFVT is known to predict the phase diagram only qualitatively when $q>1$.[16] In addition, the range κ^{-1} of the electrostatic repulsion in the systems of Fig. 18 is quite large, so that $m \geq 1.4$ [see Eq. (10)]. Note further that Kobayashi *et al.*[60] encountered difficulties in describing dispersions of nanosized silica particles quantitatively using a DLVO-like potential. Thus, our comparison of the GFVT phase diagram with the experimental data should be considered only as a first attempt to relate phase separation processes and gelation.

V. CONCLUSIONS

We have studied the aggregation kinetics and the phase behavior in aqueous mixtures of charge-stabilized silica spheres (Ludox) and nonadsorbing neutral homopolymers (dextran). By varying the polymer molar mass, and the polymer and electrolyte concentrations, we can tune the range and strength of the depletion attraction and electrostatic repulsion. In addition, the colloids strongly attract each other at very short distances due to vdW forces, which can trigger irreversible colloid aggregation depending on the height of the Coulomb barrier. For low ϕ, we have measured the time-resolved colloid cluster aggregation rate using DLS. From these measurements, we find that the formation of clusters is enhanced with increasing electrolyte and polymer concentrations, and increasing colloid volume fraction. Furthermore, we observe that the cluster aggregation rate decreases with increasing q and fixed c/c^*. We have demonstrated that the combined effects of salt-induced electrostatic screening, depletion attraction and vdW attraction on the initial colloid aggregation, can be quantitatively described for $c<c^*$ by the dimer formation theory where two-particle hydrodynamics is included. We have accounted for the screened electrostatic repulsion using an effective colloid charge determined from matching the theoretical τ_a to the experimental one, for a colloid dispersion without added polymers. The depletion attraction is described in our model calculations by the AOV potential without any adjustable parameters. Overall, the polymer influence on τ_a is well explained by the AOV dimer formation theory. For c close to c^*, however, we find that the measured aggregation rate deviates significantly from the theoretical predictions. This finding can be attributed, in particular, to the nonideal solution behavior of dextran observed for $c/c^* \approx 1$, which is not accounted for in the AOV model.

With increasing ϕ and c, and lower c_s, and several hours up to a few days after sample preparation, we observe the formation of a turbid, viscous phase at the container bottom and the formation of a fluidlike upper phase. In Figs. 16 and 18 the dividing line separating homogeneous single phase samples from samples which have either phase separated or are forming a gel, shifts to smaller values of ϕ and c with increasing observation time. This line shift is more pronounced at high electrolyte concentration due to the enlarged electrostatic screening. The experimental nonequilibrium phase behavior has been compared to the equilibrium phase diagram of a corresponding system without vdW attractions as predicted by the GFVT. We observe that all samples which have phase separated after 2 days are located within the GFVT predicted spinodal region. These samples are turbid right after sample mixing. Additional dilution experiments show that the silica particles do not irreversibly aggregate up to a few hours after sample preparation. Thus, we argue that the experimentally studied nonequilibrium phase separation process may be initiated on crossing the spinodal line. However, whether gelation is related to the initial phase separation process remains to be an interesting open question.

ACKNOWLEDGMENTS

We thank Sylvia de Waal and Hui Ning for the TEM picture, and George Petekidis and Benoit Loppinet for their encouraging interest and valuable suggestions.

APPENDIX: DIMER FORMATION THEORY OF INITIAL FLOCCULATION

Consider a dispersion which initially consists of nonaggregated colloidal spheres randomly distributed in the system volume V. Whenever two particles approach each other so that the singular short-range vdW interparticle attractions become dominant, they can form a dimer. If the dispersion is highly diluted, we can neglect three-body and higher order collision events at short times. The formation of dimers can then be described by an evolution equation for the pair probability density, $P_2(r,t)$, of finding two spheres at time t at a center-to-center distance r,[26,28]

$$\frac{\partial P_2(r,t)}{\partial t} = \frac{1}{r^2}\frac{\partial}{\partial r}\left[2D_0 G(r)\frac{\partial P_2(r,t)}{\partial r} + 2D_0 G(r) P_2(r,t)\frac{d\beta u(r)}{dr}\right], \tag{A1}$$

where $G(r)$ is the relative hydrodynamic mobility of two spheres of free diffusion coefficient D_0 along their line of centers. The first term on the right-hand side arises from the diffusive flux part, which tends to smooth out local accumulations of colloidal particles. The second term accounts for the relative flux caused by $u(r)$. At very short interparticle distances, when the vdW attraction part dominates, this term becomes negative, favoring a local accumulation of spheres. Initially, $P_2(r,0)=n_0^2$, where $n_0=n(t=0)$ is the initial number density of randomly distributed colloids (monomers). The inner and outer boundary conditions are $P_2(\infty,t)=n_0^2$ and

$P_2(2a,t)=0$, respectively, on assuming a random distribution of spheres for $r\to\infty$ and irreversible dimer formation at contact, respectively. From the solution of Eq. (A1) and the aforementioned initial and boundary conditions, the collision rate is obtained to[28]

$$J_{11}=4\pi(2a)^2\lim_{r\to 2a^+}2D_0G(r)\left[\frac{\partial P_2(r,t)}{\partial r}+P_2(r,t)\frac{d\beta u(r)}{dr}\right]. \tag{A2}$$

The time-dependent monomer number concentration, $n(t)$, is then obtained from the rate equation, $dn(t)/dt=-J_{11}$ that describes the disappearance of monomers from the suspension. Using a steady-state approximation the solution reads[28]

$$P_2(r,t)=n_0^2\frac{\exp[-\beta u(r)]\int_{2a}^{r}dr'\frac{\exp[\beta u(r')]}{r'^2G(r')}}{\int_{2a}^{\infty}dr'\frac{\exp[\beta u(r')]}{r'^2G(r')}}, \tag{A3}$$

and the collision rate follows as

$$J_{11}=\frac{8\pi D_0n_0^2}{\int_{2a}^{\infty}dr'\frac{\exp[\beta u(r')]}{r'^2G(r')}}. \tag{A4}$$

For $u(r)=0$ and $G(r)=1$, Eq. (A4) reduces to the classical result of Smoluchowski for diffusion-limited aggregation, namely, $J_0=16\pi aD_0n_0^2$. The stability ratio, W, is defined by

$$W=\frac{J_0}{J_{11}}=2a\int_{2a}^{\infty}dr\frac{\exp[\beta u(r)]}{r^2G(r)}, \tag{A5}$$

and the characteristic aggregation time, τ_a, of dimer formation is given by

$$\tau_a=\frac{\pi\eta a^3}{\phi k_BT}W. \tag{A6}$$

[1] W. C. K. Poon, J. Phys.: Condens. Matter **14**, R859 (2002).
[2] A. P. Gast, C. K. Hall, and W. B. Russel, J. Colloid Interface Sci. **96**, 251 (1983).
[3] H. Verduin and J. K. G. Dhont, J. Colloid Interface Sci. **172**, 425 (1995).
[4] N. A. M. Verhaegh, D. Asnaghi, H. N. W. Lekkerkerker, M. Giglio, and L. Cipelletti, Physica A **242**, 104 (1997).
[5] P. Poulin, J. Bibette, and D. A. Weitz, Eur. Phys. J. B **7**, 277 (1999).
[6] S. Manley, H. M. Wyss, K. Miyazaki, J. C. Conrad, V. Trappe, L. J. Kaufman, D. R. Reichman, and D. A. Weitz, Phys. Rev. Lett. **95**, 238302 (2005).
[7] P. Charbonneau and D. R. Reichman, Phys. Rev. E **75**, 011507 (2007).
[8] P. J. Lu, E. Zaccarelli, F. Ciulla, A. B. Schofield, F. Sciortino, and D. A. Weitz, Nature (London) **453**, 499 (2008).
[9] J. Bergenholtz and M. Fuchs, Phys. Rev. E **59**, 5706 (1999).
[10] J. Bergenholtz, W. C. K. Poon, and M. Fuchs, Langmuir **19**, 4493 (2003).
[11] A. M. Puertas and G. Odriozola, J. Phys. Chem. B **111**, 5564 (2007).
[12] E. Zaccarelli, J. Phys.: Condens. Matter **19**, 323101 (2007).
[13] S. Asakura and F. Oosawa, J. Chem. Phys. **22**, 1255 (1954).
[14] S. Asakura and F. Oosawa, J. Polym. Sci. **33**, 183 (1958).
[15] A. Vrij, Pure Appl. Chem. **48**, 471 (1976).
[16] C. Gögelein and R. Tuinier, Eur. Phys. J. E **27**, 171 (2008).
[17] S. Rawson, K. Ryan, and B. Vincent, Colloids Surf. **34**, 89 (1988).
[18] S. N. Sharma, A. Tan, and J. Walz, J. Colloid Interface Sci. **191**, 236 (1997).
[19] J. L. Burns, Y.-d. Yan, G. J. Jameson, and S. Biggs, J. Colloid Interface Sci. **247**, 24 (2002).
[20] R. Dunleavey-Routh and B. Vincent, J. Colloid Interface Sci. **309**, 119 (2007).
[21] J. W. Tavacoli, P. J. Dowding, and A. F. Routh, Colloids Surf., A **293**, 167 (2007).
[22] F. K. R. Li-In-On, B. Vincent, and F. A. Waite, Am. Chem. Soc. Symp. Ser. **9**, 165 (1975).
[23] B. Vincent, P. F. Lukham, and F. A. Waite, J. Colloid Interface Sci. **73**, 508 (1980).
[24] J. E. Seebergh and J. C. Berg, Langmuir **10**, 454 (1994).
[25] G. Petekidis, L. A. Galloway, S. U. Egelhaaf, M. E. Cates, and W. C. K. Poon, Langmuir **18**, 4248 (2002).
[26] W. B. Russel, D. A. Saville, and W. R. Schowalter, *Colloidal Dispersions* (Cambridge University Press, Cambridge, 1992).
[27] G. Nägele, *The Physics of Colloidal Soft Matter* (Institute of Fundamental Technological Research Publishing, Polish Academy of Sciences, Warsaw, 2004).
[28] W. B. Russel, *The Phase Behaviour and Dynamics of Colloidal Dispersions* (University of Utrecht, Utrecht, 2005).
[29] S. Kim and S. J. Karrila, *Microhydrodynamics* (Dover, Mineola, 1990).
[30] D. J. Acheson, *Elementary Fluid Dynamics* (Oxford University Press, Oxford, 1990).
[31] E. Nordmeier, J. Phys. Chem. **97**, 5770 (1993).
[32] H. N. W. Lekkerkerker, W. C. K. Poon, P. N. Pusey, A. Stroobants, and P. W. Warren, Europhys. Lett. **20**, 559 (1992).
[33] J. A. Barker and D. Henderson, J. Chem. Phys. **47**, 2856 (1967).
[34] A. Fortini, M. Dijkstra, and R. Tuinier, J. Phys.: Condens. Matter **17**, 7783 (2005).
[35] N. F. Carnahan and K. E. Starling, J. Chem. Phys. **51**, 635 (1969).
[36] K. A. Granath, J. Colloid Sci. **13**, 308 (1958).
[37] B. J. Berne and R. Pecora, *Dynamic Light Scattering* (Robert E. Krieger, Malabar, 1990).
[38] C. P. Lindsey and G. D. Patterson, J. Chem. Phys. **73**, 3348 (1980).
[39] *CRC Handbook of Chemistry and Physics*, edited by D. R. Lide (CRC, New York, 1997).
[40] A. J. Banchio and G. Nägele, J. Chem. Phys. **128**, 104903 (2008).
[41] P. N. Pusey and R. J. A. Tough, in *Dynamic Light Scattering*, edited by R. Pecora (Plenum, New York, 1985), pp. 85–179.
[42] G. Nägele, Phys. Rep. **272**, 215 (1996).
[43] A. K. van Helden, J. W. Jansen, and A. Vrij, J. Colloid Interface Sci. **81**, 354 (1981).
[44] S. Coenen and C. G. de Kruif, J. Colloid Interface Sci. **124**, 104 (1988).
[45] A. van Blaaderen and A. P. M. Kentgens, J. Non-Cryst. Solids **149**, 161 (1992).
[46] P. Sandkühler, J. Sefcik, and M. Morbidelli, J. Phys. Chem. B **108**, 20105 (2004).
[47] M. Doi and S. F. Edwards, *The Theory of Polymer Dynamics* (Oxford University Press, Oxford, 1988).
[48] G. J. Fleer, M. A. Cohen Stuart, J. M. H. M. Scheutjens, T. Cosgrove, and B. Vincent, *Polymers at Interfaces* (Springer, Berlin, 1993).
[49] X. Zeng and K. Osseo-Asare, Colloids Surf., A **226**, 45 (2003).
[50] B. A. Jucker, H. Harms, S. J. Hug, and A. J. B. Zehnder, Colloids Surf., B **9**, 331 (1997).
[51] X. Zeng and K. Osseo-Asare, J. Colloid Interface Sci. **272**, 298 (2004).
[52] D. W. Schaefer, J. E. Martin, P. Wiltzius, and D. S. Cannell, Phys. Rev. Lett. **52**, 2371 (1984).
[53] G. Dietler, C. Aubert, D. S. Cannell, and P. Wiltzius, Phys. Rev. Lett. **57**, 3117 (1986).
[54] M. Y. Lin, R. Klein, H. M. Lindsay, D. A. Weitz, R. C. Ball, and P. Meakin, J. Colloid Interface Sci. **137**, 263 (1990).
[55] B. D. Butler, C. D. Muzny, and H. J. M. Hanley, Int. J. Thermophys. **20**, 35 (1999).
[56] P. A. Heiney, R. J. Butera, J. D. Londono, R. V. Davidson, and S. Mazur, J. Phys. Chem. B **104**, 8807 (2000).
[57] H. M. Wyss, J. Innerlohinger, L. P. Meier, L. J. Gauckler, and O. Glatter, J. Colloid Interface Sci. **271**, 388 (2004).
[58] G. L. Tan, M. F. Lemon, D. J. Jones, and R. H. French, Phys. Rev. B **72**, 205117 (2005).
[59] S. Pianegonda, E. Trizac, and Y. Levin, J. Chem. Phys. **126**, 014702 (2007).
[60] M. Kobayashi, F. Juillerat, P. Galletto, P. Bowen, and M. Borkovec, Langmuir **21**, 5761 (2005).
[61] S. Y. Shulepov and G. J. Frens, J. Colloid Interface Sci. **170**, 44 (1995).
[62] S. Y. Shulepov and G. J. Frens, J. Colloid Interface Sci. **182**, 388 (1996).

[63] H. Kihira, N. Ryde, and E. Matijevic, J. Chem. Soc., Faraday Trans. **88**, 2379 (1992).
[64] G. M. Litton and T. M. Olson, J. Colloid Interface Sci. **165**, 522 (1994).
[65] J. N. Israelachvili and R. M. Pashley, Nature (London) **306**, 249 (1983).
[66] J. N. Israelachvili and H. Wennerström, Nature (London) **379**, 219 (1996).
[67] J. E. Martin, J. P. Wilcoxon, D. Schaefer, and J. Odinek, Phys. Rev. A **41**, 4379 (1990).
[68] W. B. Russel and D. W. Benzing, J. Colloid Interface Sci. **83**, 163 (1981).
[69] A. R. Denton, Phys. Rev. E **62**, 3855 (2000).
[70] S. Sauer and H. Löwen, J. Phys.: Condens. Matter **8**, L803 (1996).
[71] L. Belloni, J. Chem. Phys. **85**, 519 (1986).
[72] M. C. Grant and W. B. Russel, Phys. Rev. E **47**, 2606 (1993).